

# *Carbon budget for 1.5 and 2oC targets lowered by natural wetland and permafrost feedbacks*

Article

Accepted Version

Comyn-Platt, E., Hayman, G., Huntingford, C., Chadburn, S. E., Burke, E. J., Harper, A. B., Collins, W. J. ORCID: <https://orcid.org/0000-0002-7419-0850>, Webber, C. P., Powell, T., Cox, P. M., Gedney, N. and Sitch, S. (2018) Carbon budget for 1.5 and 2oC targets lowered by natural wetland and permafrost feedbacks. *Nature Geoscience*, 11. pp. 568-573. ISSN 1752-0894 doi: <https://doi.org/10.1038/s41561-018-0174-9> Available at <https://centaur.reading.ac.uk/77371/>

It is advisable to refer to the publisher's version if you intend to cite from the work. See [Guidance on citing](#).

To link to this article DOI: <http://dx.doi.org/10.1038/s41561-018-0174-9>

Publisher: Nature Publishing Group

All outputs in CentAUR are protected by Intellectual Property Rights law, including copyright law. Copyright and IPR is retained by the creators or other copyright holders. Terms and conditions for use of this material are defined in the [End User Agreement](#).

[www.reading.ac.uk/centaur](http://www.reading.ac.uk/centaur)

**CentAUR**

Central Archive at the University of Reading

Reading's research outputs online

# 1 **Carbon budget for 1.5 and 2°C targets lowered by natural wetland** 2 **and permafrost feedbacks**

3 Edward Comyn-Platt<sup>1,\*</sup>, Garry Hayman<sup>1</sup>, Chris Huntingford<sup>1</sup>, Sarah Chadburn<sup>2,3</sup>, Eleanor  
4 Burke<sup>4</sup>, Anna Harper<sup>3</sup>, William Collins<sup>5</sup>, Christopher Webber<sup>5</sup>, Tom Powell<sup>4</sup>, Peter Cox<sup>4</sup>, Nic  
5 Gedney<sup>6</sup>, Stephen Sitch<sup>4</sup>

6 1: Centre for Ecology and Hydrology, Wallingford, OX10 8BB, U.K.

7 2: University of Leeds, Leeds, LS2 9JT, U.K.

8 3: University of Exeter, Exeter, EX4 4QF, U.K.

9 4: Met Office Hadley Centre, FitzRoy Road, Exeter, EX1 3PB, U.K.

10 5: University of Reading, Reading, RG6 6BB, U.K.

11 6: Met Office Hadley Centre, Joint Centre for Hydrometeorological Research, Wallingford,  
12 OX10 8BB, U.K.

13 \* Corresponding Author

14 **Keywords: Climate stabilisation, global warming, temperature thresholds, carbon cycle,**  
15 **methane cycle, permafrost thaw**

16 **Methane emissions from natural wetlands and carbon release from permafrost thaw have**  
17 **a positive feedback on climate, yet are not represented in most state-of-the-art climate**  
18 **models. Furthermore, a fraction of the thawed permafrost carbon is released as methane,**  
19 **enhancing the combined feedback strength. We present simulations with an intermediate**  
20 **complexity climate model which follow prescribed global warming pathways to**  
21 **stabilisation at 1.5°C or 2.0°C above pre-industrial levels by the year 2100, and that**  
22 **incorporates a state-of-the-art global land surface model with updated descriptions of**  
23 **wetland and permafrost carbon release. We demonstrate that the climate feedbacks from**  
24 **those two processes are substantial. Specifically, permissible anthropogenic fossil fuel**  
25 **CO<sub>2</sub> emission budgets are reduced by 17-23% (47-56 GtC) for stabilisation at 1.5°C, and**  
26 **9-13% (52-57 GtC) for 2.0°C stabilisation. In our simulations these feedback processes**  
27 **respond faster at temperatures below 1.5°C, and the differences between the 1.5°C and**  
28 **2°C targets are disproportionately small. This key finding is due to our interest in**

29 **transient emission pathways to the year 2100 and does not consider the longer term**  
30 **implications of these feedback processes. We conclude that natural feedback processes**  
31 **from wetlands and permafrost must be considered in assessments of transient emission**  
32 **pathways to limit global warming.**

### 33 **Background**

34 The 2009 meeting of the United Nations' Framework Convention on Climate Change  
35 (UNFCCC) in Copenhagen formalised the aspiration to stabilise global warming at no more  
36 than 2°C above pre-industrial levels<sup>1</sup>. The subsequent UNFCCC Paris Agreement in 2015  
37 raised the additional possibility of aiming for an even lower upper warming threshold of 1.5°C<sup>2</sup>.  
38 These targets will require large reductions in anthropogenic greenhouse gas (GHG) emissions,  
39 with sustained decreases of ~3% per annum<sup>3,4</sup> and development of technologies to remove  
40 carbon dioxide (CO<sub>2</sub>) from the atmosphere. This is because the equilibrium global warming for  
41 current GHG concentrations may already be near 1.5°C<sup>5</sup>. Given the anticipated difficulty in  
42 keeping below the 1.5°C threshold, two key questions are being asked. First, what are the  
43 implications in terms of allowable anthropogenic emissions to keep warming below 1.5°C  
44 rather than 2.0°C? Second, what is gained climatically or environmentally by keeping below  
45 1.5°C, i.e. are unwelcome climate impacts potentially avoided?

46 The climate change observed during recent decades has been strongly linked to human  
47 influences on atmospheric GHG composition, leading the 5<sup>th</sup> IPCC assessment to state: “it is  
48 extremely likely that human influence has been the dominant cause of the observed warming  
49 since the mid-20<sup>th</sup> century”<sup>6</sup>. However atmospheric GHG levels are affected both directly (via  
50 anthropogenic GHG emissions) and indirectly by human activity. Indirect effects include  
51 climate change-induced adjustments to the land-atmosphere and/or ocean-atmosphere GHG  
52 exchange fluxes. This was first modelled for the global carbon cycle by [7] who predicted a

53 significant flux of carbon to the atmosphere via increased plant and soil respiration under  
54 warming for a business-as-usual scenario. Similar analyses have been undertaken separately  
55 for additional methane (CH<sub>4</sub>) release from wetlands<sup>8,9</sup> and additional carbon released from the  
56 long-term permafrost store<sup>10-12</sup>. The increase in global warming may be under-estimated for a  
57 prescribed anthropogenic emissions trajectory if these processes are not considered. In  
58 reference to policy objectives, the anthropogenic fossil fuel emission budgets (AFFEBs) to  
59 limit global warming to 1.5°C or 2.0°C may be significantly reduced from current  
60 assessments<sup>6,13,14</sup>.

61 This research focusses on two key feedback processes which were not included in most models  
62 in the fifth phase of the Coupled Model Intercomparison Project (CMIP5)<sup>15</sup> and will only be  
63 included in a small fraction of models participating the sixth phase (CMIP6). These are the  
64 effects of carbon release from the long-term permafrost store as CO<sub>2</sub> and the increased CH<sub>4</sub>  
65 emissions from natural wetlands, and the coupling between the two effects where carbon from  
66 thawed permafrost is also released as CH<sub>4</sub><sup>16,17</sup>. These are particularly pertinent issues given that  
67 CH<sub>4</sub> has a larger Global Warming Potential (GWP) by equivalent weight than CO<sub>2</sub>, and the  
68 recent resurgent growth in atmospheric CH<sub>4</sub><sup>18</sup>.

69 In contrast to CMIP5 simulations, which modelled climatic and environmental responses to  
70 prescribed pathways in atmospheric concentrations, the objective here is to estimate the  
71 anthropogenic response to meet a specified global warming target. We develop an inverted  
72 form of climate model to follow prescribed temperature trajectories<sup>19</sup> and calculate the  
73 corresponding AFFEBs<sup>13</sup>, including the two aforementioned feedback effects. The modelling  
74 framework is based on the coupled Joint UK Land Environment Simulator (JULES<sup>20,21</sup>) and  
75 Integrated Model Of Global Effects of climatic aNomalies (IMOGEN<sup>22,23</sup>) system (Methods).  
76 The approach taken is generic and may be employed in further research to answer a number of  
77 environmental policy related questions in terms of meeting specified warming thresholds.

## 78 **Model Setup**

79 We use JULES version 4.8 release, with the addition of a 14 layered soil column for both  
80 hydro-thermal<sup>24</sup> and carbon<sup>25</sup> dynamics (Methods). The JULES configuration includes  
81 representations of land-use and land-use change (LULUC) and ozone damage on plant stomata  
82 to address policy-relevant warming scenarios outside the scope of this paper. Full JULES  
83 details are given in Methods.

84 The major advancement in the IMOGEN configuration used for this study is the prescription  
85 of evolving global temperature trajectories. Following this inverted form (Figure SI.1b;  
86 Methods), changes in radiative forcing,  $\Delta Q$ , are calculated as a function of the time-history of  
87 global warming which are then ascribed to compatible atmospheric compositions of GHGs.  
88 The anthropogenic contribution to atmospheric CO<sub>2</sub> is calculated whilst taking in to account  
89 changes to the land and ocean carbon stores, together with prescription or calculation of non-  
90 CO<sub>2</sub> greenhouse gases. Additional IMOGEN enhancements for this analysis include the  
91 calculation of atmospheric CH<sub>4</sub> concentration and effective radiative forcing, capturing the  
92 climate impacts on CH<sub>4</sub> release from natural wetlands (Methods).

93 Critical to our analysis is understanding emission pathways available to stabilise at either 1.5°C  
94 or 2.0°C of warming since pre-industrial times. As this will be strongly influenced by  
95 anthropogenic perturbation of the climate system to present day, we constrain the historical  
96 global temperature ( $\Delta T_G$ ) to the HadCRUT4 observational record<sup>26</sup> and atmospheric  
97 composition to the Representative Concentration Pathway (RCP) record<sup>27</sup> for the period 1850-  
98 2015. Future projections of the non-CO<sub>2</sub> atmospheric composition is taken from the IMAGE-  
99 3.0 implementation of Shared-Socioeconomic-Pathway (SSP) version 2 under RCP2.6  
100 (SSP2\_RCP-2.6\_IMAGE)<sup>28</sup> (Methods).

101 We select three possible global warming pathways to stabilisation at the 1.5°C or 2.0°C targets  
102 by 2100 (Figure 1a and Figure SI.2), which are described using the formulation in [19]  
103 (Methods). Two of the considered trajectories follow the more traditional scenario of reaching  
104 asymptotes at 1.5°C and 2.0°C from below. The third asymptotes to 1.5°C after an overshoot  
105 to 1.75°C, representing far greater attempts of decarbonisation of the atmosphere towards the  
106 end of the 21<sup>st</sup> century. The overshoot trajectory allows investigation into hysteresis effects  
107 which may have path-dependent impact on temperature stabilisation, e.g. carbon release due to  
108 permafrost thaw.

## 109 **Discussion**

110 The atmospheric CO<sub>2</sub> concentrations and derived anthropogenic emission pathways from our  
111 control runs (i.e. with no natural wetland CH<sub>4</sub> nor permafrost carbon feedbacks) are displayed  
112 in Figure 1. Using this “standard” configuration of JULES, we estimate the interquartile range  
113 of the AFFEBs for 2015-2100 as 464-568 GtC to meet the 2°C target, and 227-283 GtC or 227-  
114 288 GtC to meet the 1.5°C target with or without the overshoot, respectively (Table 1). The  
115 AFFEBs are broadly linear in  $\Delta T_G$  across the three scenarios, i.e. 378-480 GtC °C<sup>-1</sup> and 421-  
116 516 GtC °C<sup>-1</sup> for the 1.5°C and 2°C scenarios, respectively. These results agree with previous  
117 estimates of AFFEBs using different methods<sup>13</sup>.

118 The 2°C scenario allows close to “business as usual” emissions for the coming decade followed  
119 by extensive emission reductions of 3.5-4.1% per year between 2030 and 2100. However, if  
120 society were to act more immediately, the AFFEB could be met with year-on-year reductions  
121 of 2.2-2.7% from 2020. The 1.5°C scenario with no overshoot indicates a near immediate peak  
122 in annual emissions followed by 3.5-4.3% year-on-year reductions from 2020. Despite the  
123 similarity of the AFFEB for the two 1.5°C scenarios, the overshoot scenario places larger  
124 pressure on future generations. This pathway implies that anthropogenic activities are a net

125 311-377 GtC source of CO<sub>2</sub> until the early-2050s, then must become a net sink, capturing 90.4-  
126 101 GtC. These estimates go further than previous attempts to quantify AFFEB<sup>13,14</sup> as they  
127 provide an AFFEB for each GCM, and the transient pathway, to meet the specified stabilised  
128 temperature.

129 The role of permafrost thaw in modulating the AFFEB is measured as the amount of carbon  
130 that was in the pre-industrial permafrost carbon store that is lost to the atmosphere. We define  
131 permafrost as soil layers within grid cells which JULES simulates as perennially frozen. We  
132 find our estimates of present day permafrost extent and loss rate to agree with the models  
133 assessed in [11] (Figure SI.3). Furthermore, a comparison with an observation dataset<sup>29</sup>  
134 demonstrates that our simulations reproduce a reasonable present day spatial coverage of  
135 permafrost (Figure SI.4). By 2100, the model ensemble estimates a median 138 Mha loss of  
136 permafrost area at 3m depth for the 1.5°C asymptote pathway and a median 239 Mha loss for  
137 the 2.0°C pathway (Figure 2a and Table SI.3). This degradation of permafrost results in an  
138 additional 40.0-46.3, 45.6-51.2 and 61.9-72.0 GtC of pre-industrial permafrost carbon which  
139 is no longer perennially frozen, relative to 2015, for the three temperature scenarios. Between  
140 20% and 30% of this newly “thermally active” carbon has been released to the atmosphere,  
141 reducing AFFEBs by 11.6-13.8 GtC across the three scenarios (Figure 2d and Table 1– blue  
142 boxes in first column). The uncertainty range presented here is the interquartile range of the  
143 climate ensemble. We use a model configuration very close to the upper extreme of the process  
144 uncertainty presented in [10], hence our estimates represent an upper limit to the potential  
145 permafrost feedback. Applying the findings of [10] implies that a lower limit to the permafrost  
146 feedback would be roughly half of what is presented here (~5-7 GtC).

147 The differences in permafrost loss between scenarios appears less than previous estimates<sup>30</sup>.  
148 However, our estimates represent a transient snapshot at 2100 and not equilibrium conditions  
149 which will not be met for several centuries. The permafrost is not in equilibrium by 2100,



150 particularly the deeper soil layers which show a lagged response to changes in the surface air  
151 temperature (Figure 2a and 2b). This behaviour is similarly observed in the pre-industrial  
152 permafrost carbon stocks which are still being significantly depleted by year 2100 (Figure 2c  
153 and 2d). The loss-rate of pre-industrial permafrost carbon to the atmosphere is still increasing  
154 by 2100 as the total pool of soil carbon to respire continues to grow despite the stabilisation of  
155 surface air temperature. This highlights the time-scales involved in permafrost processes and  
156 indicates that permafrost thaw will continue to have large implications on anthropogenic  
157 emissions into the 22<sup>nd</sup> century even if temperatures have stabilised.

158 The response of the AFFEB to permafrost thaw is non-linear with respect to  $\Delta T_G$ , i.e. 19.3-21.7  
159 GtC °C<sup>-1</sup> for the 1.5°C scenarios and 11.6-12.5 GtC °C<sup>-1</sup> for the 2°C scenario. This implies that  
160 the permafrost feedback is faster at lower temperature changes, and keeping temperatures  
161 below 1.5°C, rather than 2°C, does not make large differences to AFFEBs to 2100. However,  
162 this behaviour is primarily a feature of our interest in the AFFEB to 2100 and the additional  
163 carbon released in the 2°C scenario will continue to have implications into the 22<sup>nd</sup> century.

164 The impact of the natural wetland CH<sub>4</sub> feedback on the AFFEBs is the sum of reduced carbon  
165 uptake of the atmosphere, ocean and land due to a higher atmospheric CH<sub>4</sub> concentration. The  
166 magnitude and distribution of the JULES natural wetland CH<sub>4</sub> emissions are driven primarily  
167 by wetland area and the soil temperature and carbon content (Methods). Our estimates of  
168 wetland extent and zonal distribution for the present day are within the range of state-of-the-  
169 art observation datasets<sup>31,32</sup> (Figure SI.4). To encapsulate a range of methanogenesis process  
170 uncertainty we include a temperature sensitivity ensemble by varying  $Q_{10}$  in Equation 1  
171 (Methods). We use  $Q_{10}$  values calibrated to represent two wetland types identified in [33]  
172 (“poor-fen” and “rich-fen”) and a third “low- $Q_{10}$ ” which gave increased importance to high  
173 latitude emissions (Methods). Our ensemble spread sufficiently describes the magnitude and  
174 distribution of present day CH<sub>4</sub> emissions from natural wetlands according to the models

175 assessed in a recent intercomparison study<sup>34</sup> (Figure SI.5). That said, there is still much  
176 uncertainty in natural wetland CH<sub>4</sub> emissions and future work will look to improve our model  
177 via more rigorous comparisons with observational datasets.

178 The global mean atmospheric CH<sub>4</sub> concentrations are increased by 3-9% and 6-15% (w.r.t. the  
179 control simulation) when the natural CH<sub>4</sub> feedback is included for the 1.5°C and 2°C target,  
180 respectively (Figure 3a for the “poor-fen” parameterisation and supplementary Figure SI.6 for  
181 the other parameterisations). The major driver of increased CH<sub>4</sub> emissions is increased soil  
182 temperatures as changes in wetland extent and soil carbon content are not consistent globally  
183 (Figure SI.7). The increased atmospheric CH<sub>4</sub> concentrations imply reduced atmospheric CO<sub>2</sub>  
184 concentrations to ensure that simulations follow the prescribed temperature pathway (Figure  
185 3b). The reduced atmospheric CO<sub>2</sub> concentrations result in reduced CO<sub>2</sub> fertilisation of  
186 vegetation and a slower oceanic drawdown of CO<sub>2</sub>. Additionally, the increased ozone due to  
187 increased CH<sub>4</sub> (Methods) limits productivity further still. The AFFEBs are hence lowered by  
188 33-51 GtC for the full temperature sensitivity ensemble (yellow cells in Table 1 and Figure  
189 3d).

190 Similar to the permafrost feedback, the natural CH<sub>4</sub> feedback is non-linear with respect to  $\Delta T_G$ ,  
191 i.e. 55-71 GtC °C<sup>-1</sup> for the 1.5°C scenario and 34-46 GtC °C<sup>-1</sup> for the 2°C scenario. The effects  
192 of the natural CH<sub>4</sub> feedbacks are 13-21% larger for the 2°C scenario than the 1.5°C scenarios  
193 despite a temperature increase that is 83% larger, from present day. Furthermore, we found that  
194 this non-linear behaviour was maintained for the three temperature sensitivities considered in  
195 our uncertainty analysis (Figure 3d). Therefore, in the context of the natural wetland feedback  
196 strength, we conclude that constraining warming to less than 1.5°C, rather than 2°C, has a  
197 disproportionately small impact on the AFFEB.

198 The natural CH<sub>4</sub> feedback strength is slightly reduced for the 1.5°C with overshoot in  
199 comparison to the 1.5°C asymptote pathway (Figure 3a). The two scenarios have similar  
200 atmospheric CH<sub>4</sub> concentrations by 2100 (median difference < 5ppb) hence the atmospheric  
201 CO<sub>2</sub> sinks in year 2100 are similar. However, the overshooting pathway has higher atmospheric  
202 CO<sub>2</sub> concentrations during the 21<sup>st</sup> Century, hence the ocean and land sinks are not reduced by  
203 as much. This implies that an overshooting pathway may be more robust to the natural CH<sub>4</sub>  
204 feedback as the land and ocean sinks are more effective. Given that the magnitude of this  
205 difference is small, 1-2 GtC, it is difficult to generalise this behaviour.

206 Our simulations show little interaction (where thawed permafrost is released as CH<sub>4</sub>) between  
207 the feedback processes, i.e. the difference between the sum of the AFFEB differences and  
208 AFFEB difference from the simulation including both feedback processes < 2 GtC. The amount  
209 of CH<sub>4</sub> released from the thawed permafrost carbon is 0.2-0.6 TgCH<sub>4</sub> per year, where the upper  
210 limit corresponds to the “low-Q<sub>10</sub>” parameterisation (Figure SI.8a) which gave a greater  
211 emphasis to CH<sub>4</sub> emissions from cooler regions (methods). This is ~0.16-0.56 % of global CH<sub>4</sub>  
212 emissions in 2015, decreasing to ~0.12-0.46% in 2100 (Figure SI.8b). Similarly, the fraction  
213 of permafrost carbon released as CH<sub>4</sub> is 0.15-0.59% (Figure SI.8c). The additional atmospheric  
214 CH<sub>4</sub> translates to changes of global atmospheric CO<sub>2</sub> of the order 0.1 ppmv, which has little  
215 impact on the absolute atmospheric carbon sink nor the uptake of carbon by the land and ocean.  
216 Hence, in the context of our estimates of AFFEBs to meet the UNFCC targets (200-500 GtC),  
217 the interplay of these two feedback schemes is largely negligible. However, our modelling  
218 framework does not account for thermokarst lakes created via ground subsidence following  
219 permafrost thaw. To provide an estimate of uncertainty regarding this omission we emulate the  
220 behaviour offline by linearly increasing wetland extent in permafrost regions through the 21<sup>st</sup>  
221 Century, from a factor of 1 in year 2000 to a factor of 2 in year 2100 (Figure SI.10). The  
222 increased CH<sub>4</sub> emissions reduces the AFFEB by a further 0.8-2.5 GtC. However, we see this

223 as an over-estimate as the emulation does not consider the reduced aerobic respiration due to  
224 increased saturated soil which has been shown to outweigh the increased CH<sub>4</sub> emissions<sup>16</sup>.

## 225 **Conclusions**

226 The combined effect of these feedback processes has large implications on AFFEBs, 16.7-  
227 23.2% (46.6-55.7 GtC) and 9.5-13% (51.4-64.6 GtC) reductions for the 1.5°C and 2°C  
228 scenarios from the control runs, respectively (Table 1 – green cells). In terms of mitigation  
229 pathways this corresponds to 4.6-5.4% year-on-year reductions in anthropogenic emissions  
230 beginning in 2020 to meet the 1.5°C emission budget. To meet the 2°C warming target, the  
231 allowable emissions would require year-on-year reductions of 3.9-4.5% beginning in 2030, or  
232 2.4-3.0% starting in 2020. This represents a 1-1.5% increase in reduction rates for the 1.5°C  
233 and only a 0.3-0.6% increase in reduction rates for the 2°C. The 1.5°C overshoot pathway  
234 indicates that total allowable anthropogenic emissions would need to be no more than 292-351  
235 GtC prior to the mid-2050s followed by a removal of 101-118 GtC.

236 We find that to fulfil a 1.5°C warming threshold with no overshoot, increased CH<sub>4</sub> emissions  
237 from natural wetlands reduce the AFFEB between now and year 2100 by 12-17%. Carbon  
238 released from the long-term permafrost store reduces the AFFEB by an additional 4.1-5.3%,  
239 and the interplay between the two processes a further 0.5-1 %. This leaves AFFEBs of 175-  
240 235 GtC to 2100, a total reduction of 17-23%. Allowing for an overshoot to 1.75°C, but still  
241 leading ultimately to 1.5°C warming, makes little difference to the AFFEB, 172-240 GtC to  
242 2100. However, such an eventuality would require significant developments of carbon capture  
243 technologies in the second half of the 21<sup>st</sup> century during which the net anthropogenic  
244 contribution to the carbon cycle would have to be a 101-118 GtC sink. The reduction in AFFEB  
245 for stabilisation at 2.0°C is, in absolute terms, similar to the reductions required to meet the  
246 1.5°C target, 51.4-64.6 GtC. However, this is a much lower fraction of the AFFEB, 9.5-13.0%.

247 Our overall findings are that the natural climate feedbacks considered here are non-linear with  
248 respect to the AFFEB to meet a given temperature target by year 2100. Therefore, the role of  
249 the natural CH<sub>4</sub> and permafrost thaw feedback processes become increasingly more important  
250 when considering the lower stabilisation temperature target of 1.5°C.

## 251 **References**

- 252 1 UNFCCC. Copenhagen Accord FCCC/CP/2015/L.9/Rev. 1. (2009).  
253 2 UNFCCC. Adoption of the Paris Agreement FCCC/CP/2015/L.9/Rev. 1. (2015).  
254 3 Huntingford, C. *et al.* The link between a global 2 °C warming threshold and emissions in  
255 years 2020, 2050 and beyond. *Environmental Research Letters* **7**, 014039 (2012).  
256 4 Rogelj, J., McCollum, D. L., Reisinger, A., Meinshausen, M. & Riahi, K. Probabilistic  
257 cost estimates for climate change mitigation. *Nature* **493**, 79-83 (2013).  
258 5 Huntingford, C. & Mercado, L. M. High chance that current atmospheric greenhouse  
259 concentrations commit to warmings greater than 1.5 °C over land. **6**, 30294 (2016).  
260 6 IPCC. in *Climate Change 2013: The Physical Science Basis. Contribution of Working*  
261 *Group I to the Fifth Assessment Report of the Intergovernmental Panel on Climate Change*  
262 (eds T.F. Stocker *et al.*) (Cambridge University Press, 2013).  
263 7 Cox, P. M., Betts, R. A., Jones, C. D., Spall, S. A. & Totterdell, I. J. Acceleration of global  
264 warming due to carbon-cycle feedbacks in a coupled climate model. *Nature* **408**, 184-187,  
265 doi:10.1038/35041539 (2000).  
266 8 Gedney, N., Cox, P. M. & Huntingford, C. Climate feedback from wetland methane  
267 emissions. *Geophysical Research Letters* **31**, doi:10.1029/2004gl020919 (2004).  
268 9 Shindell, D. T., Walter, B. P. & Faluvegi, G. Impacts of climate change on methane  
269 emissions from wetlands. *Geophysical Research Letters* **31**, L21202,  
270 doi:10.1029/2004GL021009 (2004).  
271 10 Burke, E. J. *et al.* Quantifying uncertainties of permafrost carbon–climate feedbacks.  
272 *Biogeosciences* **14**, 3051 (2017).  
273 11 McGuire, A. D. *et al.* Variability in the sensitivity among model simulations of permafrost  
274 and carbon dynamics in the permafrost region between 1960 and 2009. *Global*  
275 *Biogeochemical Cycles* **30**, 1015-1037, doi:10.1002/2016GB005405 (2016).  
276 12 Burke, E. J., Chadburn, S. E., Huntingford, C. & Jones, C. D. CO<sub>2</sub> loss by permafrost  
277 thawing implies additional emissions reductions to limit warming to 1.5 or 2 °C.  
278 *Environmental Research Letters* **13**, 024024 (2018).  
279 13 Millar, R. J. *et al.* Emission budgets and pathways consistent with limiting warming to  
280 1.5°C. *Nature Geoscience*, 741-748, doi:10.1038/ngeo3031 (2017).  
281 14 Tokarska, K. B. & Gillett, N. P. Cumulative carbon emissions budgets consistent with  
282 1.5 °C global warming. *Nature Climate Change* **8**, 296-299, doi:10.1038/s41558-018-  
283 0118-9 (2018).  
284 15 Taylor, K. E., Stouffer, R. J. & Meehl, G. A. An Overview of CMIP5 and the Experiment  
285 Design. *Bulletin of the American Meteorological Society* **93**, 485-498, doi:10.1175/bams-  
286 d-11-00094.1 (2012).  
287 16 Schädel, C. *et al.* Potential carbon emissions dominated by carbon dioxide from thawed  
288 permafrost soils. *Nature Climate Change* **6**, 950, doi:10.1038/nclimate3054 (2016).  
289 17 Schuur, E. A. G. *et al.* Climate change and the permafrost carbon feedback. *Nature* **520**,  
290 171-179, doi:10.1038/nature14338 (2015).

- 291 18 Crill, P. M. & Thornton, B. F. Whither methane in the IPCC process? *Nature Climate*  
292 *Change* **7**, 678, doi:10.1038/nclimate3403 (2017).
- 293 19 Huntingford, C. *et al.* Flexible parameter-sparse global temperature time profiles that  
294 stabilise at 1.5 and 2.0 °C. *Earth Syst. Dynam.* **8**, 617-626, doi:10.5194/esd-8-617-2017  
295 (2017).
- 296 20 Best, M. *et al.* The Joint UK Land Environment Simulator (JULES), model description–  
297 Part 1: energy and water fluxes. *Geoscientific Model Development* **4**, 677-699 (2011).
- 298 21 Clark, D. *et al.* The Joint UK Land Environment Simulator (JULES), model description–  
299 Part 2: carbon fluxes and vegetation dynamics. *Geoscientific Model Development* **4**, 701-  
300 722 (2011).
- 301 22 Huntingford, C. & Cox, P. M. An analogue model to derive additional climate change  
302 scenarios from existing GCM simulations. *Climate Dynamics* **16**, 575-586,  
303 doi:10.1007/s003820000067 (2000).
- 304 23 Huntingford, C. *et al.* IMOGEN: an intermediate complexity model to evaluate terrestrial  
305 impacts of a changing climate. *Geoscientific Model Development* **3**, 679-687,  
306 doi:10.5194/gmd-3-679-2010 (2010).
- 307 24 Chadburn, S. *et al.* An improved representation of physical permafrost dynamics in the  
308 JULES land-surface model. *Geoscientific Model Development* **8**, 1493-1508 (2015).
- 309 25 Burke, E. J., Chadburn, S. E. & Ekici, A. A vertical representation of soil carbon in the  
310 JULES land surface scheme (vn4. 3\_permafrost) with a focus on permafrost regions.  
311 *Geoscientific Model Development* **10**, 959 (2017).
- 312 26 Morice, C. P., Kennedy, J. J., Rayner, N. A. & Jones, P. D. Quantifying uncertainties in  
313 global and regional temperature change using an ensemble of observational estimates: The  
314 HadCRUT4 data set. *Journal of Geophysical Research: Atmospheres* **117**, D08101,  
315 doi:10.1029/2011JD017187 (2012).
- 316 27 Meinshausen, M. *et al.* The RCP greenhouse gas concentrations and their extensions from  
317 1765 to 2300. *Climatic Change* **109**, 213, doi:10.1007/s10584-011-0156-z (2011).
- 318 28 van Vuuren, D. P. *et al.* Energy, land-use and greenhouse gas emissions trajectories under  
319 a green growth paradigm. *Global Environmental Change* **42**, 237-250 (2017).
- 320 29 Brown, J., Ferrians Jr, O., Heginbottom, J. & Melnikov, E. (National Snow and Ice Data  
321 Center, 1998).
- 322 30 Chadburn, S. E. *et al.* An observation-based constraint on permafrost loss as a function of  
323 global warming. **7**, 340, doi:10.1038/nclimate3262 (2017).
- 324 31 Zhang, B. *et al.* Methane emissions from global wetlands: An assessment of the  
325 uncertainty associated with various wetland extent data sets. *Atmospheric Environment*  
326 **165**, 310-321, doi:<https://doi.org/10.1016/j.atmosenv.2017.07.001> (2017).
- 327 32 Poulter, B. *et al.* Global wetland contribution to 2000–2012 atmospheric methane growth  
328 rate dynamics. *Environmental Research Letters* **12**, 094013 (2017).
- 329 33 Turetsky, M. R. *et al.* A synthesis of methane emissions from 71 northern, temperate, and  
330 subtropical wetlands. *Global Change Biology* **20**, 2183-2197, doi:10.1111/gcb.12580  
331 (2014).
- 332 34 Saunio, M. *et al.* The global methane budget 2000–2012. *Earth Syst. Sci. Data* **8**, 697-  
333 751, doi:10.5194/essd-8-697-2016 (2016).
- 334 35 Jones, C. *et al.* The HadGEM2-ES implementation of CMIP5 centennial simulations.  
335 *Geoscientific Model Development* **4**, 543 (2011).
- 336 36 Zona, D. *et al.* Cold season emissions dominate the Arctic tundra methane budget.  
337 *Proceedings of the National Academy of Sciences* **113**, 40-45,  
338 doi:10.1073/pnas.1516017113 (2016).
- 339 37 McNorton, J. *et al.* Role of regional wetland emissions in atmospheric methane variability.  
340 *Geophysical Research Letters* **43**, 11,433-411,444, doi:10.1002/2016GL070649 (2016).

- 341 38 Clark, D. *et al.* The Joint UK Land Environment Simulator (JULES), model description -  
342 Part 2: Carbon fluxes and vegetation dynamics. *Geoscientific Model Development* **4**, 701-  
343 722, doi:10.5194/gmd-4-701-2011 (2011).
- 344 39 Gedney, N. & Cox, P. M. The sensitivity of global climate model simulations to the  
345 representation of soil moisture heterogeneity. *Journal of Hydrometeorology* **4**, 1265-1275  
346 (2003).
- 347 40 Marthews, T., Dadson, S., Lehner, B., Abele, S. & Gedney, N. High-resolution global  
348 topographic index values for use in large-scale hydrological modelling. *Hydrology and*  
349 *Earth System Sciences* **19**, 91-104 (2015).
- 350 41 Klein Goldewijk, K., Beusen, A., Van Drecht, G. & De Vos, M. The HYDE 3.1 spatially  
351 explicit database of human-induced global land-use change over the past 12,000 years.  
352 *Global Ecology and Biogeography* **20**, 73-86 (2011).
- 353 42 Sitch, S., Cox, P. M., Collins, W. J. & Huntingford, C. Indirect radiative forcing of climate  
354 change through ozone effects on the land-carbon sink. *Nature* **448**, 791-794 (2007).
- 355 43 Stohl, A. *et al.* Evaluating the climate and air quality impacts of short-lived pollutants.  
356 *Atmos. Chem. Phys.* **15**, 10529-10566, doi:10.5194/acp-15-10529-2015 (2015).
- 357 44 Etminan, M., Myhre, G., Highwood, E. J. & Shine, K. P. Radiative forcing of carbon  
358 dioxide, methane, and nitrous oxide: A significant revision of the methane radiative  
359 forcing. *Geophysical Research Letters* **43**, 12,614-612,623, doi:10.1002/2016GL071930  
360 (2016).
- 361 45 IPCC. *Climate change 2001: the scientific basis*. (The Press Syndicate of the University  
362 of Cambridge, 2001).

### 363 **Corresponding Author**

364 All correspondence and requests for materials should be made to Edward Comyn-Platt  
365 (edwcom@ceh.ac.uk).

### 366 **Acknowledgements**

367 The work was undertaken as part of the UK Natural Environment Research Council's  
368 programme "Understanding the Pathways to and Impacts of a 1.5°C Rise in Global  
369 Temperature" through grants NE/P015050/1 CLIFFTOP (E.C-P, G.H., S.C.), NE/P014909/1,  
370 MOC1.5 (W.C., C.W., C.H., P.C., S.S.) and NE/P014941/1 CLUES (P.C., T.P.). We also  
371 acknowledge the support for: (a) E.B. and N.G., the Joint UK BEIS/Defra Met Office Hadley  
372 Centre Climate Programme (GA01101); (b) E.B., CRESCENDO (EU project 641816); (c)  
373 A.H., EPSRC Fellowship "Negative Emissions and the Food-Energy-Water Nexus"  
374 (EP/N030141/1); and (d) C.H., CEH National Capability Funding. We also acknowledge the

375 wetland extent data products provided by Dr. B. Zhang, of Auburn University, USA and Dr.  
376 B. Poulter of the NASA Goddard Space Flight Center, USA.

### 377 **Author Contributions**

378 G.H., E.B., S.C. and E.C-P conceived and developed the project. E.C-P and C.H. led the  
379 development of the inverse IMOGEN model system. E.B. and S.C. contributed code and  
380 expertise on permafrost and soil carbon modelling. N.G., S.C. and E.C.P. contributed code and  
381 expertise on the JULES wetlands methane scheme. A.H. and T.P. contributed land use change,  
382 W.C. and C.W. ozone ancillary data and S.S. contributed expertise on the ozone damage  
383 effects, respectively. E.C-P., C.H., G.H., E.B., S.C., W.C., C.W., P.C., A.H. and T.P.  
384 contributed to the design of the IMOGEN model runs. All authors contributed to the  
385 interpretation of the results and to the writing of the paper.

### 386 **Competing financial interests**

387 The authors declare no competing financial interests.



## 388 **Methods**

### 389 **(1) The JULES model<sup>20,21</sup>.**

#### 390 **(a) Model version and configuration**

391 JULES is a process-based land surface model that simulates energy, water and carbon fluxes  
392 at the land-atmosphere boundary. JULES can be run as a standalone model using given  
393 meteorological driving variables or as the land surface component of climate modelling  
394 systems of varying degrees of complexity, e.g. Earth System Models<sup>35</sup> or IMOGEN<sup>18</sup>. We use  
395 the JULES version 4.8 release with the addition of a 14 layered soil column over 3m for both  
396 hydro-thermal<sup>24</sup> and carbon dynamics<sup>25</sup>. Burke et al.,<sup>25</sup> demonstrated that modelling the soil  
397 carbon fluxes as a multi-layered scheme improves estimates of soil carbon stocks and net  
398 ecosystem exchange. In addition to the vertically discretised respiration and litter input terms,  
399 the soil carbon balance also includes a diffusivity term which represents  
400 cryoturbation/bioturbation processes. The freeze-thaw processes of cryoturbation is  
401 particularly important in cold permafrost type soils<sup>10</sup>.

402 The multi-layered methanogenesis scheme improves the representation of high latitude CH<sub>4</sub>  
403 emissions where previous studies underestimated production at cold permafrost sites during  
404 “shoulder seasons”<sup>36</sup>. The multi-layered scheme allows an insulated sub-surface layer of active  
405 methanogenesis to continue after the surface has frozen. These model developments not only  
406 improve the seasonality of the emissions, but more importantly for this study capture the release  
407 of carbon as CH<sub>4</sub> from deep soil layers, including thawed permafrost. The formulation of the  
408 multi-layered scheme gives the local land-atmosphere CH<sub>4</sub> flux,  $E_{CH_4}$  (kg C m<sup>-2</sup> s<sup>-1</sup>), as:

$$E_{CH_4} = k \cdot f_{wetl} \cdot \sum_{C_s \text{ pools}}^i \kappa_i \cdot \sum_{z=0m}^{z=3m} e^{-\gamma z} C_{S_{i,z}} \cdot Q_{10}(T_{soil_z})^{0.1(T_{soil_z}-T_0)}$$

Equation 1

409 Where  $z$  is the depth in soil column (in  $m$ ),  $i$  is the soil carbon pool,  $f_{wetl}$  (-) is the fraction of  
410 wetland area in the gridcell,  $\kappa_i$  ( $s^{-1}$ ) is the specific respiration rate of each pool (Table 8 of [21]),  
411  $C_s$  ( $kg\ m^{-2}$ ) is soil carbon,  $T_{soil}$  (K) is the soil temperature.  $\gamma$  ( $= 0.4\ m^{-1}$ ) is a constant that  
412 describes the reduced contribution of  $CH_4$  emission at deeper soil layers due to inhibited  
413 transport and increased oxidation through overlaying soil layers. This is a simplification,  
414 however previous work which explicitly represented these processes showed little to no  
415 improvement when compared with in-situ observations<sup>37</sup>. The four soil carbon pools ( $i$ ) in  
416 JULES are decomposable plant material, resistant plant material, microbial biomass, and  
417 humus. As JULES is a processed based model, the carbon emitted as  $CH_4$  is therefore removed  
418 from the soil carbon stock. Furthermore, as described in [38], soil respiration is non-zero in  
419 fully saturated soils, hence in anaerobic conditions JULES produces  $CO_2$  in addition to  $CH_4$ .

420  $f_{wetl}$  is calculated using the JULES implementation of TOPMODEL<sup>39</sup> as the integral of a  
421 normalised gamma distribution of a prescribed topographic index dataset<sup>40</sup>,  $G(\tau)$ , between a  
422 critical,  $\tau_{crit}$  ( $\ln(m)$ ), and maximum,  $\tau_{max}$  ( $\ln(m)$ ), topographic index, i.e.:

$$f_{wetl} = \int_{\tau_{crit}}^{\tau_{max}} G(\tau) d\tau, \quad \text{Equation 2}$$

423  $\tau_{crit}$  is dependent on the local water table as:

$$\tau_{crit} = \ln\left(\frac{\Psi(0)}{\Psi(\bar{z}_w)}\right) + \bar{\tau}, \quad \text{Equation 3}$$

424 where  $\Psi(0)$  and  $\Psi(\bar{z}_w)$  ( $m^2s^{-1}$ ) are the transmissivities of entire soil column and the soil column  
425 below the mean water table depth,  $\bar{z}_w$  ( $m$ ). The  $\tau_{max}$  limit excludes regions where the water  
426 table is sufficiently high enough for stream flow and hence assumed to be a negligible emitter  
427 of  $CH_4$ . It is calculated as:

$$\tau_{max} = \tau_{crit} + \tau_{range}, \quad \text{Equation 4}$$

428 where  $\tau_{range}$  ( $= 2.0$ ) is a global tuning parameter.

429  $\bar{z}_w$  is incrementally updated based on the balance of water flux processes on each JULES  
 430 timestep. When  $\bar{z}_w$  is in the deep store (a singular 15 m below the 14 modelled layers) it is  
 431 updated as the balance between the infiltration water,  $I_{Deep}$ , and the baseflow,  $B_{Deep}$ , as:

$$\rho\theta_{sat} \frac{d(\bar{z}_w)}{dt} = I_{Deep} - B_{Deep}, \quad \text{Equation 5}$$

432 where  $\rho$  is the density of water and  $\theta_{sat}$  is the saturated volumetric water content. If the deep  
 433 layer is fully saturated  $\bar{z}_w$  is calculated diagnostically to be in the deepest unsaturated model  
 434 soil layer. The water content of each layer,  $j$ , is updated on each time step as the balance of the  
 435 vertical flux processes (infiltration,  $I_j$ , and Evapotranspiration,  $E_j$ ), and, for layers below  $\bar{z}_w$ , a  
 436 horizontal baseflow flux,  $B_j$ , i.e.:

$$\Delta z_j \rho \frac{d(\theta_j)}{dt} = I_j - E_j - B_j, \quad \text{Equation 6}$$

437 where  $\Delta z_j$  is the thickness and  $\theta_j$  is the volumetric water content of  $j^{\text{th}}$  soil layer. For full details  
 438 of the process based JULES hydrology please refer to [20] and [39].

439 In addition, the JULES configuration includes prescribed land-use and land-use change  
 440 (LULUC), where land used for agriculture can only grow C3 and C4 grasses to represent crops  
 441 and pasture. The land-use mask consists of an annual fraction of agricultural land in each grid  
 442 cell. Historical LULUC is based on the HYDE 3.1 dataset<sup>41</sup>, and future LULUC is based on  
 443 the SSP2\_RCP-2.6\_IMAGE<sup>28</sup>. When natural vegetation is converted to managed agricultural  
 444 land, the removed vegetation carbon is placed into woody product pools that decay at various  
 445 rates back into the atmosphere<sup>35</sup>. The carbon flux from LULUC is therefore not lost from the  
 446 system.

447 We use a JULES configuration including ozone deposition damage to plant stomata, which  
 448 then affects land-atmosphere CO<sub>2</sub> exchange<sup>42</sup>. JULES requires surface atmospheric ozone  
 449 concentrations, O<sub>3</sub> (ppb), for the duration of the simulation period (1850-2100). Here, we use

450 two sets of monthly O<sub>3</sub> concentration fields calculated using the HADGEM3-A GA4.0 model  
451 for low (1285 ppbv) and high (2062 ppbv) global mean atmospheric CH<sub>4</sub> concentrations<sup>43</sup>. We  
452 regrid these fields (1.875°x1.25° horizontal grid) to the spatial grid of IMOGEN-JULES  
453 (3.75°x2.5° horizontal grid). We then linearly interpolate between the respective months in the  
454 regridded O<sub>3</sub> fields using the global annual atmospheric CH<sub>4</sub> concentration. The CH<sub>4</sub>  
455 concentration is taken from the prescribed SSP2\_RCP-2.6\_IMAGE plus the natural CH<sub>4</sub>  
456 modulation when the interactive scheme is in use.

#### 457 **(b) Wetland CH<sub>4</sub> emission scheme calibration**

458 We calibrate the temperature sensitivity of the multi-layered methanogenesis scheme ( $k$  and  
459  $Q_{10}(T_{soil}) = Q_{10}^{[T_0/T_{soil}]}$  in Equation 1) for each CMIP5 model in the IMOGEN ensemble to  
460 ensure the wetland CH<sub>4</sub> production rates match present day observations<sup>33,34</sup>. [33] fit observed  
461 surface CH<sub>4</sub> fluxes,  $E_{CH_4}$ , against temperature to Equation 7 using data from 71 sites:

$$E_{CH_4, Turetsky} = A_{Turetsky} \times Q_{10, Turetsky}^{0.1T_{soil-10cm}}, \quad \text{Equation 7}$$

462 where  $T_{soil-10cm}$  is the temperature of the top 10 cm of soil.

463 To capture temperature sensitivity uncertainty we calibrate  $Q_{10}$  in Equation 1 against Equation  
464 7 for 2 of the wetland types identified in [33] (“Poor Fen” and “Rich Fen”) using the daily output  
465 from the JULES-simulations at the year 2000 for each GCM. We select  $Q_{10}$  values which  
466 maximise the Pearson’s correlation coefficient.  $k$  is then calculated such that the global total  
467 for the year 2000 is 180 TgCH<sub>4</sub> to match our assumptions of the atmospheric growth rate of  
468 CH<sub>4</sub> in the IMOGEN CH<sub>4</sub> feedback calculations (see IMOGEN description below). We  
469 selected the “Poor Fen” and “Rich Fen” parameterisations for our ensemble as these gave the  
470 best representation of the global distribution of CH<sub>4</sub> emissions when compared with the output  
471 from [34] (Figure SI.9). A “Bog” parameterisation was ruled out as this tended towards  
472 unrealistically high tropical emissions, a “Swamp” parameterisation was ruled out due to the

473 high levels of uncertainty reported in [33]. The optimised parameter values are given in Table  
474 SI.2 of the Supplementary Information. In addition to the two calibrated parameterisations we  
475 include a “low $Q_{10}$ ” ( $Q_{10}=2.0$ ,  $k=1.625\times 10^{-9}$ ) parameterisation which gave a larger fraction of  
476 global emissions to lower temperature regions (Figure SI.9).

477 **(2) IMOGEN, EBM Inversion and the CMIP5 models selected for its calibration.**

478 **(a) IMOGEN<sup>23</sup>** is a climate-carbon cycle model of intermediate complexity that uses “pattern-  
479 scaling” of the seven meteorological variables required to drive JULES. Huntingford, et al. <sup>23</sup>  
480 assume that changes in local temperature, precipitation, humidity, wind-speed, surface  
481 shortwave and longwave radiation and pressure are linear in global warming. Patterns are  
482 multiplied by the amount of global warming over land,  $\Delta T_L$ , to give local monthly predictions  
483 of climate change. When using IMOGEN in forward mode,  $\Delta T_L$  is calculated with an Energy  
484 Balance Model (EBM) as a function of the overall changes in radiative forcing,  $\Delta Q$  ( $\text{W m}^{-2}$ ).  
485  $\Delta Q$  is the sum of the atmospheric greenhouse gas contributions<sup>44</sup>, updated on a yearly timestep.  
486 Our simulations include a  $\text{CH}_4$  feedback system that captures the climate impacts on  $\text{CH}_4$   
487 emissions from natural wetland sources. The approach here follows that of [8] where prescribed  
488  $\text{CH}_4$  concentrations, which assume a non-varying natural wetland  $\text{CH}_4$  component<sup>28</sup>, are  
489 perturbed using the anomaly in modelled natural wetland  $\text{CH}_4$  emission. To ensure consistency  
490 with the observed atmospheric  $\text{CH}_4$  growth rate we calibrate our model to produce 180  $\text{TgCH}_4$   
491 per year for the year 2000, as detailed in the model calibration description above. The  
492 increased/reduced atmospheric  $\text{CH}_4$  concentration will have corresponding longer/short  
493 atmospheric lifetime,  $\lambda$ , than the prescribed concentration pathway. We account for changes in  
494  $\lambda$  following the formulation and parameterisation of [45], i.e.  $\lambda=8.4 \text{ yr}^{-1}$  for an atmospheric  $\text{CH}_4$   
495 concentration of 1745ppb. The changes in radiative forcing were calculated using the  
496 formulation in [44]. There is large uncertainty in the natural wetland contribution to global  $\text{CH}_4$

497 emissions, for this study we scale to 180 TgCH<sub>4</sub> per year, approximation based on a recent  
 498 model intercomparison study<sup>34</sup> (Figure SI.6). Additionally, the effect of increased atmospheric  
 499 CH<sub>4</sub> concentrations on tropospheric ozone levels is also accounted for, both in terms of  
 500 radiative forcing and the impact on surface functioning through stomatal damage (see JULES  
 501 description in Methods section 1a).

502 Previous IMOGEN studies<sup>23,10</sup> used 22 of the Earth System models (ESMs) involved in CMIP3  
 503 (phase 3 of the Coupled Model Intercomparison Project). Here, we update and extend  
 504 IMOGEN to use Earth System models (ESMs) involved in CMIP5. We downloaded CMIP5  
 505 data from the mirror database held on the UK JASMIN computer during Autumn 2015. Table  
 506 SI.1 lists every model for which historical monthly *surface temperature* fields were available.

507 The key criteria for inclusion of the output from a given CMIP5 GCM simulation is as follows  
 508 (see Supplementary Information and Table SI.1):

- 509 1. Availability for the internal Energy Balance Model of surface temperature, top of the  
 510 atmosphere (TOA) incoming shortwave radiation, outgoing TOA shortwave and longwave  
 511 radiation;
- 512 2. Availability of meteorological parameters to drive JULES: surface temperature,  
 513 precipitation, surface relative humidity, surface downward shortwave radiation, surface  
 514 downward longwave radiation, surface wind speeds and surface pressure
- 515 3. Availability of two RCP scenarios for calibration and testing

516 **(b) Energy Balance Model (EBM) Inversion.** The EBM was inverted such that a change in  
 517 radiative forcing,  $\Delta Q$ , is calculated as a function of a change in the global temperature,  $\Delta T_g$   
 518 (K), re-ordering of Equation (10) from Huntingford and Cox<sup>22</sup> gives:

$$\Delta Q(t) = f \left[ \Delta T_o \left[ \frac{(1-f)\lambda_l \nu}{f} + \lambda_o \right] - \kappa \frac{\partial \Delta T_{o,s}}{\partial z} \Big|_{z=0} \right], \quad \text{Equation 8}$$

519 Where  $\Delta Q(t)$  is the change in radiative forcing ( $\text{W m}^{-2}$ ) at time  $t$ ,  $f$  is the fraction of Earth that  
 520 is ocean,  $\lambda_l$  and  $\lambda_o$  are the climate sensitivities over land and ocean, respectively ( $\text{W m}^{-2} \text{K}^{-1}$ ),  $\nu$   
 521 is the land-sea contrast and  $\kappa$  is the ocean diffusivity ( $\text{W m}^{-1} \text{K}^{-1}$ ). The values of the parameters  
 522  $f$ ,  $\lambda_l$ ,  $\lambda_o$ ,  $\nu$  and  $\kappa$  are unique to each GCM in the ensemble and are listed in the Supplementary  
 523 Information, Table SI.2.

524 The change in the depth-dependent ocean temperature ( $\Delta T_o$ ) (K) must satisfy the diffusivity  
 525 equation:

$$c_p \frac{\partial \Delta T_{o,s}}{\partial t} = \kappa \frac{\partial^2 \Delta T_{o,s}}{\partial z^2}, \quad \text{Equation 9}$$

526 where  $c_p$  is ( $\text{J K}^{-1} \text{m}^{-3}$ ) is the specific heat capacity of salt water and  $z$  (m) is ocean depth  
 527 (positive downwards). The change in the global mean surface ocean temperature ( $z=0$ ) is then  
 528 calculated from the global temperature,  $\Delta T_G$  as <sup>22</sup>:

$$\Delta T_o = \frac{\Delta T_G}{[f + \nu - f\nu]}. \quad \text{Equation 10}$$

529 The global mean land temperature,  $\Delta T_L$ , required for the ‘‘pattern scaling’’ was calculated as:

$$\Delta T_L = \nu \Delta T_o \quad \text{Equation 11}$$

### 530 (c) Etminan CO<sub>2</sub> Radiative Forcing Inversion.

531 Etminan et al.<sup>44</sup> present a formulation to calculate the change in radiative forcing,  $\Delta Q_{CO_2}$ , from  
 532 a given change in the global mean atmospheric CO<sub>2</sub> concentration. There is no exact solution  
 533 for the inverse of this, i.e. to calculate the change in CO<sub>2</sub> for a given  $\Delta Q_{CO_2}$ . We find the solution  
 534 iteratively using Equation 3:

$$CO_{2i+1} = CO_{2\text{REF}} \times e^{\left[ \frac{\Delta Q_{CO_2}}{a_1(CO_{2i} - CO_{2\text{REF}})^2 + b_1(CO_{2i} - CO_{2\text{REF}}) + c_1\bar{N} + 5.36} \right]} \quad \text{Equation 12}$$

535 We assume convergence has occurred if the CO<sub>2</sub> concentration changes by less than 0.001  
536 ppm. The initial CO<sub>2</sub> concentration for the iteration is taken to be the CO<sub>2</sub> concentration for  
537 the previous year. We typically find that no more than 5 iterations are required for a change of  
538 10 ppm from the starting concentration.

539 **(d) Q non-CO<sub>2</sub> calculation.** Changes in radiative forcing,  $\Delta Q$  (Wm<sup>-2</sup>), calculated by the  
540 inverted IMOGEN EBM must be ascribed to changes in the atmospheric composition of GHGs.  
541 For this simplified description we consider two forcing contributions. The CO<sub>2</sub> forcing,  $\Delta Q_{CO_2}$   
542 (Wm<sup>-2</sup>), and the forcing of all other agents,  $\Delta Q_{nonCO_2}$  (Wm<sup>-2</sup>). In the simplest case (not  
543 considering interactive CH<sub>4</sub>), a prescribed  $\Delta Q_{nonCO_2}$ , is removed from  $\Delta Q$  to give  $\Delta Q_{CO_2}$  as:

$$\Delta Q_{CO_2} = \Delta Q - \Delta Q_{non\ CO_2}. \quad \text{Equation 13}$$

544 The non-CO<sub>2</sub> composition is taken from the SSP2\_RCP-2.6\_IMAGE pathway<sup>28</sup>. The  
545 SSP2\_RCP-2.6\_IMAGE pathway was chosen as it assumes very high GHG mitigation and the  
546 global warming pathway is reasonably close to the 1.5°C or 2.0°C targets of interest (i.e. 1.8  
547 °C by 2100). This prescribed non-CO<sub>2</sub> radiative forcing is subtracted from  $\Delta Q$  to give the CO<sub>2</sub>  
548 radiative forcing ( $\Delta Q_{CO_2} = \Delta Q - \Delta Q_{non\ CO_2}$ ). The CO<sub>2</sub> concentration is then derived using an  
549 iterated inversion of the CO<sub>2</sub> radiative forcing equation in Etminan et al.<sup>44</sup> (Methods). For a  
550 given  $\Delta Q_{non\ CO_2}$ , we then estimate the CO<sub>2</sub> concentration iteratively, as described above, using  
551 Equation 3.

552 Each of the 34 GCMs that IMOGEN emulates has a different set of EBM parameters -  $\lambda_1$ ,  $\lambda_o$ ,  $\nu$ ,  
553  $\kappa$  and  $f$ . Hence each GCM has a different  $\Delta Q$  estimate for a given  $\Delta T_G(t)$  pathway. When  
554 IMOGEN is driven with a historical record of  $\Delta T_G$  the range of  $\Delta Q$  for the present day (2015)  
555 is 1.13 W m<sup>-2</sup> (Supplementary Information Figure SI.5a). For this work, we require the  
556 historical period, 1850-2015, to match observations of both  $\Delta T_G$  and atmospheric composition  
557 for all GCMs. We, therefore, attribute the spread in  $\Delta Q$  to uncertainty in  $\Delta Q_{non\ CO_2}$ , particularly



558 the atmospheric aerosol contribution which has an uncertainty range of -0.5 to -4 Wm<sup>-2.6</sup>. Given  
 559 this, and to ensure continuous functions of  $\Delta Q_{CO_2}$  and  $\Delta Q_{non\ CO_2}$ , we calculated the contributions  
 560 as:

$$\Delta Q_{CO_2}(t) = \begin{cases} \Delta Q_{CO_2}(t)_{SSP}, & t \leq 2015 \\ \Delta Q(t) - \Delta Q_{non\ CO_2}(t), & t > 2015 \end{cases}$$

$$\Delta Q_{non\ CO_2}(t) = \begin{cases} \Delta Q(t) - \Delta Q_{CO_2}(t)_{SSP}, & t \leq 2015 \\ \Delta Q_{non\ CO_2}(t)_{SSP} + c(GCM), & t > 2015 \end{cases}$$

Equation 14

561 where the subscript SSP indicates the value is sourced from SSP2\_RCP-2.6\_IMAGE.  $c$  (Wm<sup>-2</sup>)  
 562 <sup>2</sup>) is a GCM specific offset which ensured continuous  $\Delta Q_{CO_2}$  or  $\Delta Q_{non\ CO_2}$  and was calculated  
 563 at the transitional year (2015) as:

$$c(GCM) = \Delta Q_{non\ CO_2}(2015) - \Delta Q_{non\ CO_2}(2015)_{SSP}$$

Equation 15

564 Figure SI.5 in the supplementary information shows the allocation of the  $\Delta Q$  and the resultant  
 565 atmospheric CO<sub>2</sub> concentration pathways for the 2°C stabilisation temperature. We include the  
 566 GCM specific 2015 aerosol-offsets in Table SI.2 in the Supplementary Information.

567 **(3) Temperature Profile Formulation.** [19] provides a framework to create temperature  
 568 trajectories based on two parameters which model the efforts of humanity to limit emissions  
 569 and, if necessary, capture atmospheric carbon, i.e.:

$$\Delta T(t) = \Delta T_0 + \gamma t + (1 - e^{-\mu(t)t})[\gamma t - (\Delta T_{Lim} - \Delta T_0)]$$

Equation 16

570 where,  $\Delta T(t)$  is the change in temperature from pre-industrial levels at year  $t$ ,  $\Delta T_0$  is the  
 571 temperature change at a given initial point (in this case  $\Delta T_0 = 0.89^\circ\text{C}$  for 2015),  $\Delta T_{Lim}$  is the  
 572 final prescribed warming limit and:

$$\mu(t) = \mu_0 + \mu_1 t,$$

Equation 17

$$\gamma = \beta - \mu_0(\Delta T_{\text{Lim}} - \Delta T_0).$$

573 Where  $\beta$  ( $= 0.00128$ ) is the current rate of warming and the  $\mu_0$  and  $\mu_1$  are tuning parameters  
 574 which describe anthropogenic attempts to stabilise global temperatures<sup>19</sup>. The selected  
 575 parameterisation of the three trajectories are based on comparisons with CMIP5 simulations  
 576 for the RCP2.6 scenario (grey lines in Figure SI.2). The parameter values used for the three  
 577 profiles selected are shown below.

Profile	$\Delta T_{\text{lim}}$	$\mu_0$	$\mu_1$
1.5°C	1.5	0.1	0.0
1.5°C (overshoot)	1.5	-0.01	0.00085
2°C	2.0	0.08	0.0

578

#### 579 (4) Code and Data Availability

580 The data that support the findings of this study are available from the corresponding author  
 581 upon request. The IMOGEN patterns and the model output required to produce the resulted  
 582 presented herein will shortly be made publicly available for download on the EIDC.

583 JULES is an open-source model and the branch used in this work is available from the met-  
 584 office science repository using the following URL (registration required):

585 [https://code.metoffice.gov.uk/trac/jules/browser/main/branches/dev/edwardcomynplatt/vn4.8\\_1P5\\_DEGREES?rev=11764](https://code.metoffice.gov.uk/trac/jules/browser/main/branches/dev/edwardcomynplatt/vn4.8_1P5_DEGREES?rev=11764)

587 The parameterisations used here are also permanently stored on the met-office science  
 588 repository. Given the complexities in accessing the specific revision and machine  
 589 configuration, these will be made available upon request to the corresponding author.

590

591 **Figures**

592

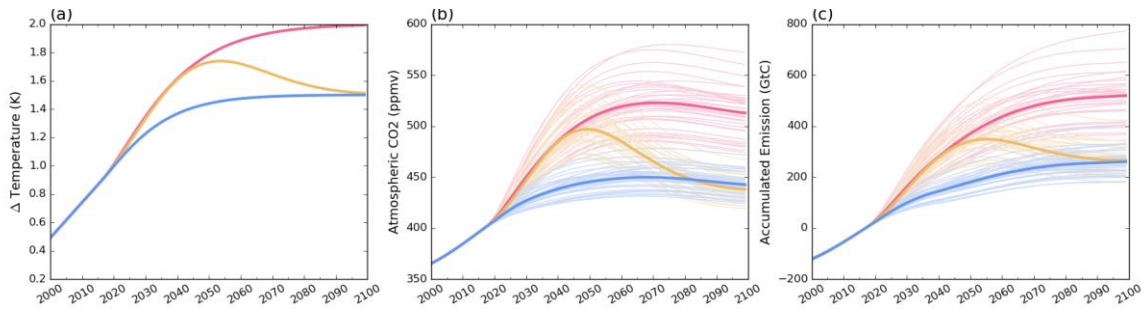


Figure 1 Time-series for the control model ensemble. Blue is the 1.5°C asymptote pathway, yellow is the 1.5°C overshoot pathway and red is the 2°C asymptote pathway. Faint lines are the individual GCMs, bold lines represent the ensemble median, and the colours are consistent across the panels. (a) Temperature pathways; (b) simulated atmospheric CO<sub>2</sub> concentrations; (c) derived allowable anthropogenic emissions.

593

594

595

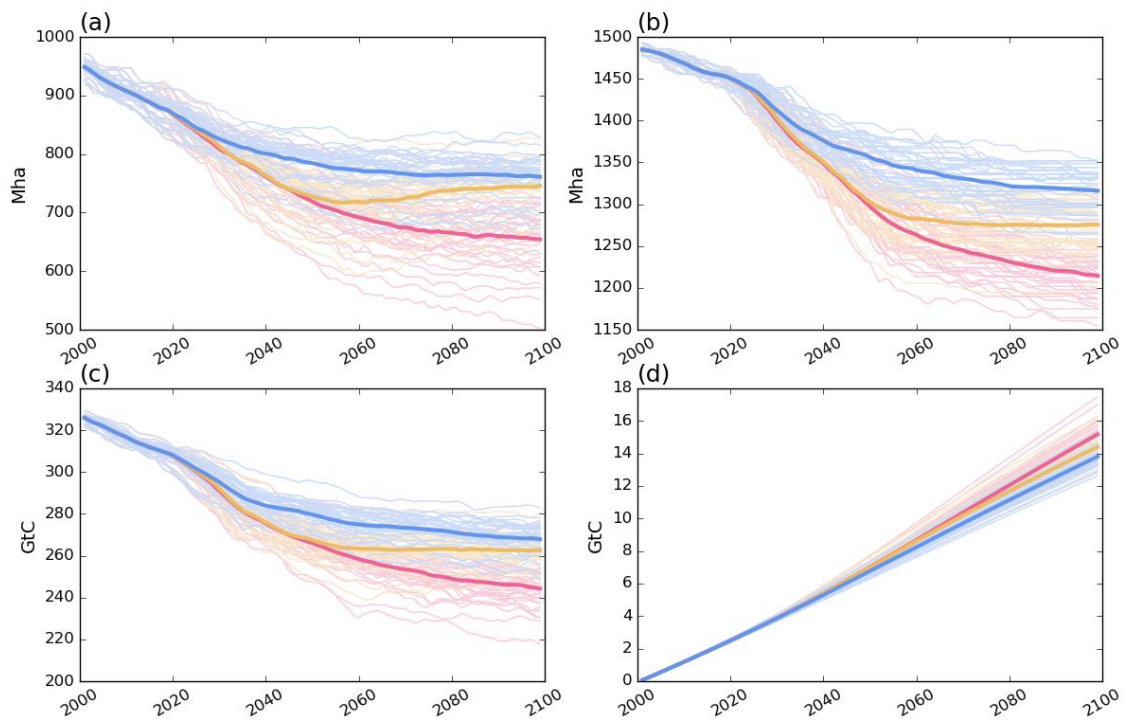


Figure 2 The response of the permafrost soil column to warming through the 21<sup>st</sup> century. (a) Areal extent of permafrost within the top 1m of soil column; (b) areal extent of permafrost within the top 3m of soil column; (c) the amount of pre-industrial permafrost carbon still perennially frozen; (d) the amount of pre-industrial carbon lost to the atmosphere. Blue is the 1.5°C asymptote pathway, yellow is the 1.5°C overshoot pathway and red is the 2°C asymptote pathway

596

597

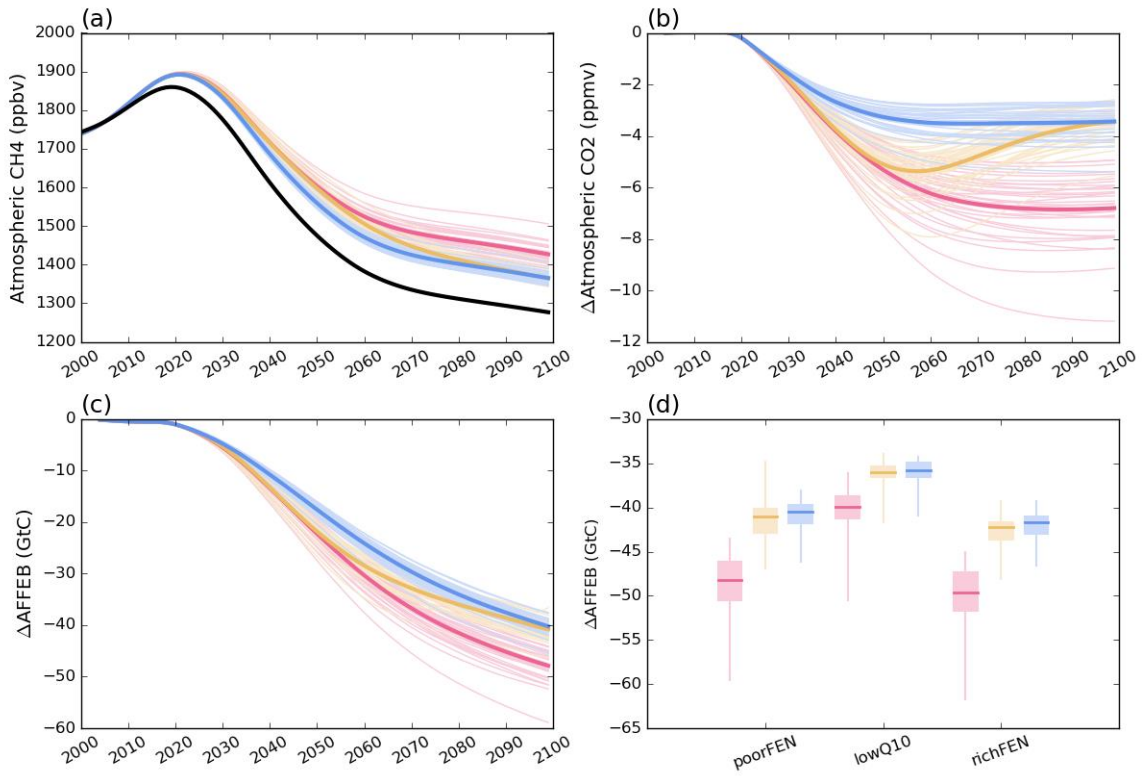


Figure 3 Summary results for the natural methane feedback experiment. (a) Time-series of atmospheric CH<sub>4</sub> when the interactive natural CH<sub>4</sub> is included (“poor fen” parameterisation) for the three temperature pathways. The black line is the control simulation atmospheric CH<sub>4</sub>. (b) The reduction in atmospheric CO<sub>2</sub> (from control simulation) to follow the prescribed temperature pathway. (c) The reduction in anthropogenic fossil fuel emissions due to reduced atmosphere, land and ocean sinks. (d) The reduction in AFFEB for the temperature sensitivity uncertainty ensemble. Blue is the 1.5°C asymptote pathway, yellow is the 1.5°C overshoot pathway and red is the 2°C asymptote pathway.

<b>Total Anthropogenic CO<sub>2</sub> emissions (GtC)</b>				
		Standard	Methane Feedback	Difference
1.5°C	Standard	<b>265</b> (226-283)	<b>226</b> (187-249)	<b>39.6</b> (33.1-42.1)
	Permafrost Feedback	<b>254</b> (214-276)	<b>214</b> (175-235)	<b>40.1</b> (34.7-42.4)
	Difference	<b>11.9</b> (11.6-12.2)	<b>12.5</b> (11.9-14.0)	<b>52.1</b> (46.6-54.2) <b>19.4 %</b> (16.7-22.9 %)
1.5°C overshoot	Standard	<b>271</b> (227-288)	<b>232</b> (185-254)	<b>40.2</b> (33.6-42.8)
	Permafrost Feedback	<b>258</b> (214-276)	<b>218</b> (172-240)	<b>40.6</b> (36.3-43.1)
	Difference	<b>12.5</b> (12.1-13.0)	<b>13.0</b> (12.4-14.3)	<b>53.5</b> (47.4-55.7) <b>19.5 %</b> (16.6-23.2 %)
2°C	Standard	<b>527</b> (464-568)	<b>504</b> (417-528)	<b>47.4</b> (37.3-51.0)
	Permafrost Feedback	<b>514</b> (451-554)	<b>467</b> (404-514)	<b>47.8</b> (38.6-51.3)
	Difference	<b>13.3</b> (12.8-13.8)	<b>13.6</b> (13.0-15.0)	<b>61.1</b> (51.4 -64.6) <b>11.4 %</b> (9.5-13.0 %)

Table 1 Emission budgets from the factorial experiment and the changes due to the introduction of the feedback processes. White cells represent the absolute emission budget for the 2015-2100 period, blue cells represent the change due to inclusion of carbon released from the permafrost store, yellow cells represent the change due to inclusion of an interactive CH<sub>4</sub> scheme and green cells represent the change due to inclusion of both permafrost and interactive CH<sub>4</sub> feedbacks. Bold values give the climate ensemble median for the “poor fen” CH<sub>4</sub> parameterisation. Bracketed values represent the spread of the climate ensemble interquartile ranges for the 3 temperature sensitivity experiments (i.e. the full spread of the boxes in Figure 3b).